Dynamic Modelling Requirements for Tuning of Cascaded Voltage and Current Loops in VSMs

Shuan Dong and Yu Christine Chen
Department of Electrical and Computer Engineering
The University of British Columbia, Vancouver, BC, Canada
Email: shuan@ece.ubc.ca, chen@ece.ubc.ca

Abstract—**This paper identifies the importance of considering the full-order virtual synchronous machine (VSM) dynamics while tuning parameters in its cascaded voltage and current control loops. Via a numerical example, we highlight that the conventional tuning method of the voltage and current loops may not ensure system stability. This is because the tuning method does not consider full-order system dynamics. Thus, we improve the tuning method for the VSM voltage and current loops using small-signal analysis of the full-order VSM model. The proposed tuning method ensures system stability in the small-signal sense, and it is computationally inexpensive. We verify the effectiveness of the proposed tuning method via numerical simulations.**

I. Introduction

Growing environmental concerns are driving terrestrial and shipboard power systems to transition from fossil fuels to renewables, e.g., wind and solar [1], [2], buffered by battery storage. The increasing share of converter-interfaced energy sources is reshaping power system dynamics, and it is challenging stable grid operation in both terrestrial and shipboard power systems. In this regard, grid-forming voltage source converters (VSCs) have been extensively studied as they can provide virtual inertia and help to stabilize the power system [3]–[12]. Grid-forming converters typically adopt droop control, virtual synchronous machine (VSM), or virtual oscillator control [13]. Among them, the VSM aims to improve power system dynamic performance by emulating dynamics of a synchronous machine.

Cascaded voltage and current control loops are included in most VSM designs, since they help to limit fault current, dampen potential resonance and improve output current quality [14]. However, the voltage and current loops introduce four additional proportional-integral (PI) controller parameters that present challenges for tuning. The conventional method to tune the voltage and current loops in [15] aims to maximize their phase margin. Ill-advised PI controller parameters in the voltage and current loops may deteriorate the system dynamic performance and even lead to instability in the worst case [9], [11]. In this paper, we demonstrate via a numerical example that such undesired results of the conventional tuning method arise because it does not consider full-order VSM dynamics.

There are two major technical routes to overcome the aforementioned shortcoming in the conventional tuning method in [15] for the voltage and current loops. The first is to redesign the VSM voltage and current loops so that they have greater achievable bandwidth and can be tuned independently.

In this vein, [16] replaces the voltage and current loops with a model predictive controller, and [10] redesigns these loops with the active disturbance rejection control. However, these designs either make system stability analysis difficult or complicate the controller design. An alternative solution is to seek improvements over the conventional tuning method of the standard voltage and current loops in [15]. For example, the tuning method in [8] considers the full-order VSM dynamics, but it requires cumbersome trial-and-error efforts. The tuning method proposed in [4] based on the eigenvalue parameter sensitivities requires less trial-and-error effort, but it may exhibit oscillatory behaviour and converge to desired PI controller parameters slowly. The method proposed in [12] searches for desired PI controller parameters with the genetic algorithm. However, this method requires manually selected parameter ranges as inputs, and it is also computationally expensive.

Contributions in this paper are summarized as follows. First, we identify the shortcoming in conventional tuning method for the voltage and current loops. That is, the conventional method does not consider the full-order VSM model and thus cannot ensure the stability of the entire system. Indeed, we identify the necessity of considering of the full-order VSM dynamics while tuning its voltage and current loops. Then, by performing small-signal analysis on the full-order VSM model, we examine the impacts of the PI controller parameters in voltage and current loops on the system dynamics. Finally, based on the small-signal analysis results, we propose a parameter tuning method for the VSM voltage and current loop. The key improvement over the conventional method is to set the integral controller parameter to be zero and choose a larger proportional controller parameter value in the voltage loop. The proposed tuning method ensures the system stability in the small-signal sense, and it is computationally inexpensive.

II. Preliminaries

This section overviews the mathematical modelling of VSM with the cascaded voltage and current control loops. Then we provide a brief description of the conventional tuning method for the VSM voltage and current control loops, which does not consider full-order VSM dynamics. Finally, via a numerical example, we demonstrate that the conventional tuning method may lead to instability.
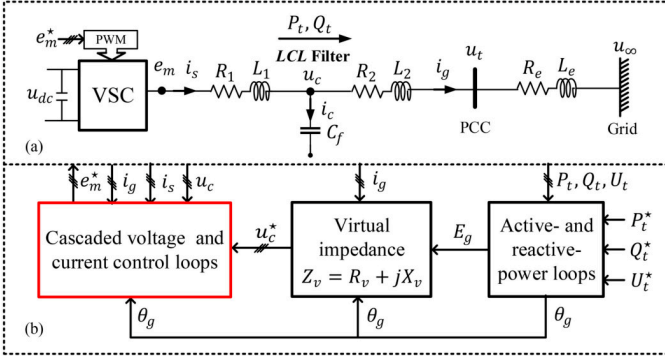
Fig. 1. VSM-connected system with cascaded voltage and current control loops. (a) Grid interface. (b) Active- and reactive-power loops, virtual impedance, and cascaded voltage and current control loops.

A. Virtual Synchronous Machine Model

As shown in Fig. 1, the VSM-connected system model typically consists of the grid interface, active- and reactive-power loops, the virtual impedance, and cascaded voltage and current control loops.

1) Grid interface: The VSC in Fig. 1(a) is connected to the grid via an LCL filter. Let e_m, u_c, and u_∞, respectively, denote the VSC AC-side terminal voltage, the VSM output voltage (i.e., the voltage across the filter capacitor C_f), and the grid-side voltage. Further let i_s, i_c, and i_g, respectively, denote the currents flowing through the converter-side filter inductor L_1 (with parasitic resistance R_1), the filter capacitor C_f, and the grid-side filter inductor L_2. Then, in the d-q reference frame, we express the dynamics of the LCL filter and the transmission line as follows:

$$e_{md} = u_{cd} - \omega_\infty L_1 i_{sq} + L_1 \frac{di_{sd}}{dt} + R_1 i_{sd}, \tag{1}$$

$$e_{mq} = u_{cq} + \omega_\infty L_1 i_{sd} + L_1 \frac{di_{sq}}{dt} + R_1 i_{sq}, \tag{2}$$

$$i_{sd} = i_{gd} - \omega_\infty C_f u_{cq} + C_f \frac{du_{cd}}{dt}, \tag{3}$$

$$i_{sq} = i_{gq} + \omega_\infty C_f u_{cd} + C_f \frac{du_{cq}}{dt}, \tag{4}$$

$$u_{cd} = u_{\infty d} - \omega_\infty (L_2 + L_e) i_{gq} + (L_2 + L_e)\frac{di_{gd}}{dt}$$
$$+ (R_2 + R_e) i_{gd}, \tag{5}$$

$$u_{cq} = u_{\infty q} + \omega_\infty (L_2 + L_e) i_{gd} + (L_2 + L_e)\frac{di_{gq}}{dt}$$
$$+ (R_2 + R_e) i_{gq}, \tag{6}$$

where ω_∞ is the grid frequency, and subscripts d and q, respectively, represent the d-axis and q-axis components.

2) Active- and reactive-power loops and virtual impedance: In Fig. 1(b), the active- and reactive-power loops regulate the VSM active-power output P_t and its reactive-power output Q_t to track their references $P_t^\star$ and $Q_t^\star$, respectively. Alternatively, they are able to achieve frequency- and voltage-droop controls based on predefined frequency and voltage references, i.e., $\omega_g^\star$ and $U_t^\star$. These regulation actions are achieved by varying the rotor angle θ_g and the voltage magnitude E_g. Also, the virtual

impedance branch $Z_v := R_v + jX_v$ can be adopted to reshape the VSM output impedance as follows:

$$u_{cd}^\star = \omega_g \psi_f - R_v i_{gd} + X_v i_{gq}, \tag{7}$$

$$u_{cq}^\star = -R_v i_{gq} - X_v i_{gd}, \tag{8}$$

where ω_g is the VSM rotating speed, ψ_f is the VSM excitation flux, and their product $E_g := \omega_g \psi_f$ represents the voltage magnitude reference generated by the power loops. In (7) and (8), $u_{cd}^\star$ and $u_{cq}^\star$ are, respectively, the d- and q-axis references of the VSM output voltage u_c. According to [5]–[7], the dynamics of the VSM power loops in Fig. 1(b) are governed by the following time-domain dynamics:

$$J_g \frac{d\omega_g}{dt} = \frac{P_t^\star}{\omega_N} - T_{ef} - D_p(\omega_g - \omega_g^\star) - D_f \frac{d}{dt}\left(\frac{T_{ef}}{\psi_{ff}}\right), \tag{9}$$

$$\frac{d\theta_{g\infty}}{dt} = \omega_g - \omega_\infty, \tag{10}$$

$$K_g \frac{d\psi_f}{dt} = Q_t^\star - Q_{tf} + \sqrt{\frac{2}{3}} D_q(U_t^\star - U_{tf}), \tag{11}$$

$$\tau_f \frac{d\psi_{ff}}{dt} = \psi_f - \psi_{ff}, \qquad \tau_f \frac{dT_{ef}}{dt} = \frac{P_t}{\omega_N} - T_{ef}, \tag{12}$$

$$\tau_f \frac{dQ_{tf}}{dt} = Q_t - Q_{tf}, \qquad \tau_f \frac{dU_{tf}}{dt} = U_t - U_{tf}, \tag{13}$$

where ω_N denotes the rated angular frequency, $\theta_{g\infty}$ denotes the phase-angle difference between the VSC AC-side terminal voltage e_m and the grid voltage u_∞, and J_g, D_p, D_f, τ_f, K_g, and D_q are tuneable controller parameters. In (9)–(13), ψ_{ff}, T_{ef}, U_{tf}, and Q_{tf} are filtered signals of the excitation flux ψ_f, the electromagnetic torque $T_e := P_t/\omega_N$, the reactive power Q_t, and the grid-side voltage magnitude U_t. Among these signals, P_t, Q_t, and U_t can be approximated by

$$P_t \approx \frac{3}{2}(u_{cd}i_{gd} + u_{cq}i_{gq}), \ Q_t \approx \frac{3}{2}(u_{cq}i_{gd} - u_{cd}i_{gq}), \tag{14}$$

$$U_t \approx \sqrt{\frac{3}{2}}\sqrt{u_{cd}^2 + u_{cq}^2}. \tag{15}$$

3) Cascaded voltage and current control loops: The control loops highlighted in red in Fig. 1(b) ensure that the filter capacitor voltage u_c closely tracks its reference value $u_c^\star$, which is generated by the active- and reactive-power loops and the virtual impedance. Specifically, as detailed in Fig. 2, the current control loop includes PI controllers as follows:

$$e_{md}^\star = u_{cd} - \omega_N L_1 i_{sq} + \frac{k_{pc}s + k_{ic}}{s}(i_{sd}^\star - i_{sd}), \tag{16}$$

$$e_{mq}^\star = u_{cq} + \omega_N L_1 i_{sd} + \frac{k_{pc}s + k_{ic}}{s}(i_{sq}^\star - i_{sq}), \tag{17}$$

where $e_{md}^\star$ and $e_{mq}^\star$ are the reference signals that serve as inputs to the pulse width modulation (PWM), and $i_{sd}^\star$ and $i_{sq}^\star$ are the reference signals of the current control loop. Likewise, the voltage control loop also includes PI controllers described by the following dynamics:

$$i_{sd}^\star = i_{gd} - \omega_N C_f u_{cq} + \frac{k_{pv}s + k_{iv}}{s}(u_{cd}^\star - u_{cd}), \tag{18}$$

$$i_{sq}^\star = i_{gq} + \omega_N C_f u_{cd} + \frac{k_{pv}s + k_{iv}}{s}(u_{cq}^\star - u_{cq}). \tag{19}$$
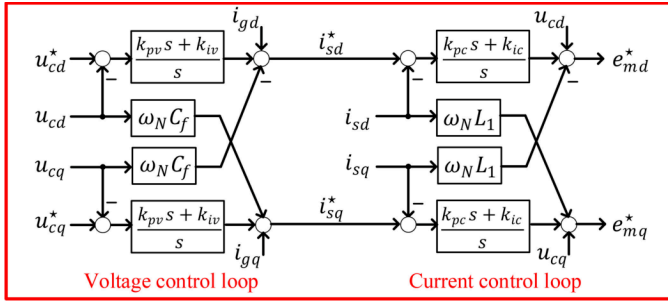
Fig. 2. Cascaded voltage and current control loops.
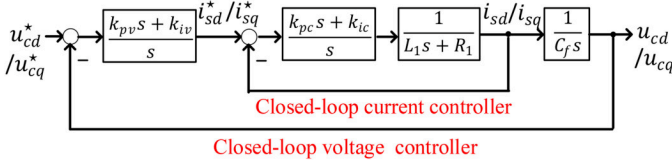
Fig. 3. Block diagram of closed-loop voltage and current control systems.

In the VSM voltage and current control loops, there are four PI controller parameters to be tuned: k_{pc}, k_{ic}, k_{pv}, and k_{iv}.

B. Conventional Tuning Method of Voltage and Current Loops

Based on (1)–(4) and (16)–(19), we obtain the block diagram representation of the closed-loop voltage and current control systems, as shown in Fig. 3. Note that the conventional tuning method does not consider the virtual impedance or the active- and reactive-power loops. Targeted at obtaining fast dynamics and achieving desired phase margin, the conventional method tunes the cascaded voltage and current control loops based on the *modulus and symmetrical optimum criteria* [15].

1) Current controller tuning via modulus optimum: Assume that $e^\star_{md} \approx e_{md}$ and $e^\star_{mq} \approx e_{mq}$, take the Laplace transform of (1) and (2), and subtract the resultant from (16) and (17), respectively. We get the following open-loop transfer funtion $G_c(s)$ of the current control dynamics:

$$G_c(s) = \frac{k_{pc}s + k_{ic}}{s} \cdot \frac{1}{L_1 s + R_1}. \qquad (20)$$

Set the desired time constant of the closed-loop system in Fig. 3 to be τ_c, and the conventional modulus optimum method computes PI parameters k_{pc} and k_{ic} from

$$k_{pc} = \frac{L_1}{\tau_c}, \quad k_{ic} = \frac{R_1}{\tau_c}. \qquad (21)$$

Then the zero in the PI controller $z = -\frac{k_{ic}}{k_{pc}}$ cancels the slower pole $s = -\frac{R_1}{L_1}$ in the filter inductor dynamics. The resultant closed-loop transfer function of the current control dynamics becomes

$$\frac{i_{sd}}{i^\star_{sd}} = \frac{i_{sq}}{i^\star_{sq}} = \frac{G_c(s)}{1 + G_c(s)} = \frac{1}{\tau_c s + 1}. \qquad (22)$$

Note that τ_c should take a small value in order to achieve fast current dynamics. At the same time, the minimum value of τ_c depends on the VSM switching frequency f_{sw}. The value of τ_c is typically chosen within the range $[0.5, 5]$ ms [15].

TABLE I
PARAMETERS OF VSM-CONNECTED SYSTEM IN EXAMPLE 1

Parameters	Values	Parameters	Values
R_1	1.4 Ω	L_1	25 mH
R_2	0.38 Ω	L_2	6.7 mH
R_e	1.4 Ω	L_e	39 mH
R_v	0	L_v	0
R_f	7.7 Ω	C_f	1.4 μF
D_p	1407 $\frac{\text{N·m·s}}{\text{rad}}$	J_g	38 kg· m^2
D_q	0	K	23333 $\frac{\text{Var·rad}}{\text{V}}$
$\omega_N, \omega^\star_g$	377 $\frac{\text{rad}}{\text{s}}$	U_∞	13.8 kVrms
f_{sw}	5.0 kHz	rated voltage	13.8 kVrms
rated capacity	1.0 MVA	DC-link voltage	25 kV

2) Voltage controller tuning via symmetrical optimum: With the well-tuned current control in place, the open-loop transfer function of the voltage control system is

$$G_v(s) = \frac{k_{pv}s + k_{iv}}{s} \cdot \frac{1}{\tau_c s + 1} \cdot \frac{1}{C_f s}, \qquad (23)$$

which has two poles at $s = 0$. The conventional symmetrical optimum method tunes PI parameters k_{pv} and k_{iv} so that $G_v(s)$ achieves desired phase margin δ_m, which is typically selected within the range $[30°, 75°]$ [15]. After specifying δ_m, k_{pv} and k_{iv} are respectively given by

$$k_{pv} = \omega_c C_f, \quad k_{iv} = \omega^3_c \tau_c C_f, \qquad (24)$$

where ω_c is the gain crossover frequency of $G_v(s)$

$$\omega_c = \frac{1}{\tau_c}\sqrt{\frac{1 - \sin \delta_m}{1 + \sin \delta_m}}. \qquad (25)$$

Next, via a numerical example, we find that the conventional tuning method above may result in instability of the VSM-connected system.

Example 1 (Examining Conventional Tuning Method). In this example (case I), we check whether or not the conventional tuning method for the cascaded voltage and current loops leads to desired VSM dynamics. We simulate the VSM-connected system in Fig. 1 in PSCAD/EMTDC using the system parameter values reported in Table I. Without loss of generality, we set the VSM virtual impedance $Z_v = 0$ and adopt the well-tuned VSM active- and reactive-power loops with the settling time 0.2 s [5]–[7]. In this case, we tune the PI parameters k_{pc}, k_{ic}, k_{pv}, and k_{iv} based on the conventional voltage and current loop tuning method. Specifically, by setting $\tau_c = 1.0$ ms and $\delta_m = 45°$ in (21), (24), and (25), we have $k_{pc} = 25$, $k_{ic} = 1406$, $k_{pv} = 5.8 \times 10^{-4}$, and $k_{iv} = 0.10$. With these PI parameter values in place, we first check the step response of the voltage and current loop in Fig. 2. As shown in Fig. 4(a), the settling time of the voltage and current loops is about 15 ms, which is over 13 times smaller than that of the outer power loops, i.e., 0.2 s. However, by simulating the active-power step response of the VSM in Fig. 1 and plotting the active power P_t in Fig. 4(b), we find that P_t does not stabilize at its reference value 1 p.u. Note that P_t remains
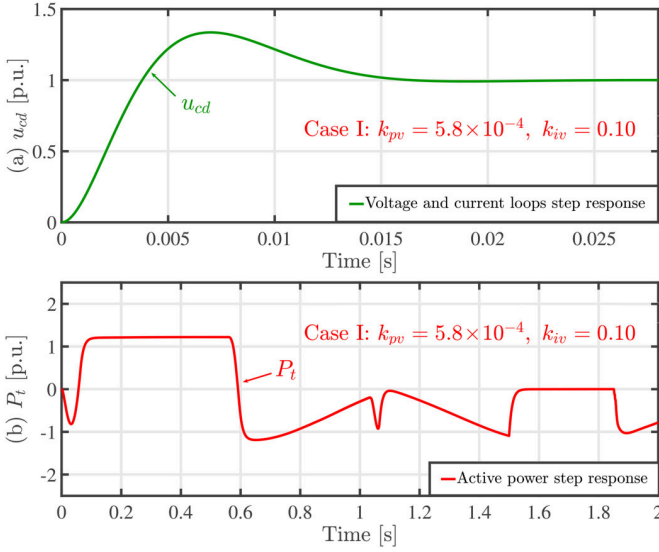
Fig. 4. System dynamics with $k_{pv} = 5.8 \times 10^{-4}$ and $k_{iv} = 0.10$ (case I). (a) Step response of cascaded voltage and current loops in Fig. 3. (b) Active-power step response of the VSM-connected system in Fig. 4.

bounded only due to the presence of current limiters. Indeed, we observe similar behaviour with other δ_m within $[30°, 75°]$. Thus, the PI parameters tuned based on conventional method destabilize the VSM-connected system in this case. ∎

C. Problem Statement

As shown in Example 1, the cascaded voltage and current loops tuned based on the conventional method do not ensure the stability of the VSM-connected system. This is because the conventional tuning method only considers the dynamics of the voltage and current control loops. Although the outer power loops are associated with slower dynamics, they cannot be neglected when tuning the voltage and current loops with faster dynamics. Next, we verify the necessity of considering the full-order system model through detailed small-signal analysis.

III. IMPROVED TUNING METHOD

This section first validates the necessity of considering the full-order system model while tuning the cascaded voltage and current loops. This is achieved by observing eigenvalues of the full-order system model. Then we show the impacts of the voltage controller PI parameters on system eigenvalues, and accordingly, propose an updated parameter tuning method for the cascaded voltage and current loops.

The VSM-connected system in Fig. 1 is fully characterized by the 17th-order nonlinear dynamical model in (1)–(15). Linearization around the equilibrium point $x°$ leads to the following small-signal state-space model:

$$\frac{d\Delta x}{dt} = A\Delta x + B\Delta u, \tag{26}$$

λ_k	Value of λ_k	λ_k	Value of λ_k
$\lambda_{1,2}$	$29.463 \pm j34.461$	$\lambda_{3,4}$	-595.61 ± 3625.1
$\lambda_{5,6}$	$-613.46 \pm j4365.6$	$\lambda_{7,8}$	-14.839 ± 26.403
$\lambda_{9,10}$	$-21.390 \pm j8.0502$	$\lambda_{11,12}$	-100.00
$\lambda_{13,14}$	-56.240	λ_{15}	-97.969
λ_{16}	-101.75	λ_{17}	-35.269
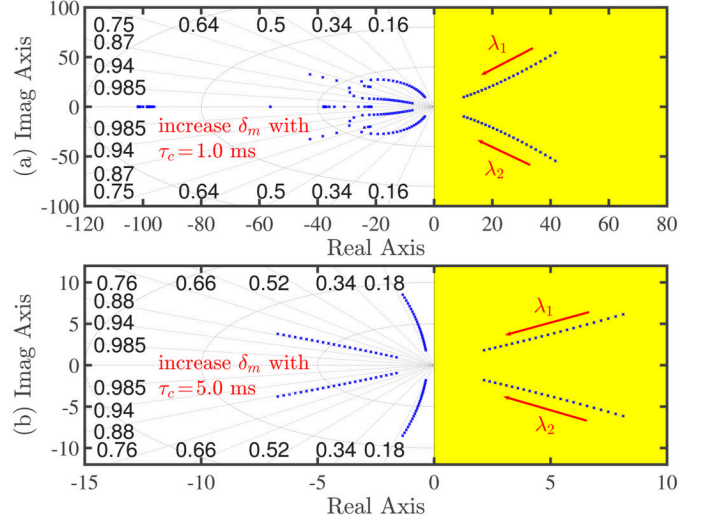
Fig. 5. Eigenvalues of full-order VSM model. (a) δ_m increases from $30°$ to $75°$ with $\tau_c = 1.0$ ms. (b) δ_m increases from $30°$ to $75°$ with $\tau_c = 5.0$ ms.

where the state vector Δx and the input vector Δu are

$$\Delta x = [\Delta\omega_g, \Delta\theta_{g\infty}, \Delta\psi_f, \Delta\psi_{ff}, \Delta T_{ef}, \Delta Q_{tf}, \Delta U_{tf}, \Delta i_{sd},$$
$$\Delta i_{sq}, \Delta u_{cd}, \Delta u_{cq}, \Delta i_{gd}, \Delta i_{gq}, \Delta\gamma_d, \Delta\gamma_q, \Delta\xi_d, \Delta\xi_q]^T,$$
$$\Delta u = [\Delta P_t^\star, \Delta Q_t^\star, \Delta U_t^\star, \Delta\omega_g^\star, \Delta\omega_\infty]^T, \tag{27}$$

respectively, with $\Delta(\cdot)$ representing small variations of the variable around its equilibrium. Note that (26) includes auxiliary variables γ_d, γ_q, ξ_d, and ξ_q to represent the states of the integrators in (16)–(19). Denote the eigenvalues of the state matrix A by λ_k, $k = 1, ..., 17$.

A. Necessity of Considering Full-order System Model

The full-order system model in (26) accurately captures the unstable dynamics of the VSM-connected system observed in Fig. 4(b). For the system in Example 1, its eigenvalues λ_k are reported in Table II. Indeed, a pair of complex-conjugate eigenvalues, i.e., λ_1 and λ_2, has positive real part, in agreement with the instability observed in Fig. 4(b). However, the conventional tuning method in Section II-B only captures the 4th-order voltage and current control system shown in Fig. 3, and thus, does not fully capture the behaviour of the entire system. We find that in Example 1, although the conventional method tunes the 4th-order voltage and current control system to be stable by setting the phase margin to be $\delta_m = 45°$, the overall VSM-connected system is unstable. Indeed, this is also true for all δ_m in the typical range $[30°, 75°]$. To see this, we increase δ_m from $30°$ to $75°$ (τ_c is fixed at 1.0 and 5.0 ms),
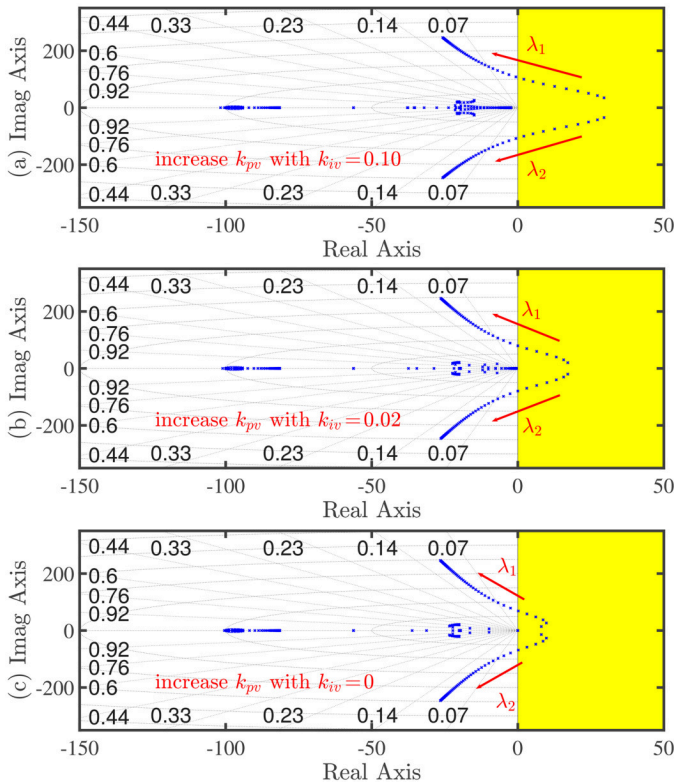
Fig. 6. Eigenvalues of full-order VSM model. (a) k_{pv} increases from 0.0006 to 0.044 with $k_{iv} = 0.40$ ($k_{pc} = 25$, $k_{ic} = 1406$). (b) k_{pv} increases from 0.0006 to 0.044 with $k_{iv} = 0.10$ ($k_{pc} = 25$, $k_{ic} = 1406$). (c) k_{pv} increases from 0.0006 to 0.044 with $k_{iv} = 0$ ($k_{pc} = 25$, $k_{ic} = 1406$).

compute k_{pv} and k_{iv} according to (24), and plot the resultant eigenvalues λ_k of the matrix $\boldsymbol{A}$ in Figs. 5(a) and 5(b). It can be found that the eigenvalues λ_1 and λ_2 lie in the right-half s-plane, and thus, the VSM-connected system is unstable. Based on the observations above, we conclude that the full-order system model in (26) should be considered when tuning the voltage and current loops.

B. Impact of Voltage Controller PI Parameters k_{pv} and k_{iv}

By observing the impact of k_{pv} and k_{iv} on eigenvalues λ_1 and λ_2, we find that increasing k_{pv} or reducing k_{iv} tends to stabilize the VSM-connected system. In Figs. 6(a), 6(b), and 6(c), we sketch three families of root loci when k_{pv} increases with different choices of k_{iv}. Note that we retain the current loop PI parameters, i.e., $k_{pc} = 25$ and $k_{ic} = 1406$. By visually inspecting each subfigure, we observe that increasing k_{pv} tends to move λ_1 and λ_2 to the left-half s-plane when k_{iv} takes different values. Also, by comparing the root loci in Figs. 6(a), 6(b), and 6(c), we find that reducing k_{iv} also enables eigenvalues λ_1 and λ_2 to migrate toward the left-half plane. This suggests that increasing the proportional parameter k_{pv} or decreasing the integral parameter k_{iv} in the voltage control loop tends to stabilize the VSM-connected system. However, the conventional tuning method from [15] and as described in Section II-B results in simultaneous increase or decrease in k_{pv} and k_{iv} to achieve desired phase margin δ_m within its typical range $[30°, 75°]$.

C. Updated Parameter Tuning Method

Based on observations in Sections III-A and III-B, we improve the voltage controller tuning method in Section II-B2 while the current controller tuning method in Section II-B1 may remain unchanged. Since reducing k_{iv} in the voltage controller improves the VSM stability, we propose to set $k_{iv} = 0$ directly, thereby reducing the voltage controller to a proportional controller. Note that the voltage signals u_{cd} and u_{cq} still track their references $u_{cd}^\star$ and $u_{cq}^\star$, respectively because the resultant open-loop transfer function of the voltage control system becomes

$$G_v(s) = k_{pv} \cdot \frac{1}{\tau_c s + 1} \cdot \frac{1}{C_f s}, \tag{28}$$

which has a pole at the origin. According to (28), the voltage control system still tracks step input without any steady-state error [17].

As observed in Section III-B, larger value for k_{pv} in the voltage controller is needed to stabilize the VSM-connected system. Thus, we may increase k_{pv} until eigenvalues λ_1 and λ_2 move into the left-half s-plane. In this way, we identify the minimum value of k_{pv}, denoted by $k_{pv}^{\min}$. Setting the parameter k_{pv} to a value greater than $k_{pv}^{\min}$ then ensures stability of the VSM-connected system.

In summary, we propose to tune the PI parameters k_{pc}, k_{ic}, k_{pv}, and k_{iv} in cascaded voltage and current loops as follows. First, we tune the current controller as in Section II-B1. Specifically, we specify a current controller time constant τ_c within its typical range $[0.5, 5]$ ms and then compute parameters k_{pc} and k_{ic} according to (21). Next, we set the voltage controller integral parameter k_{iv} to be zero. Then, we identify the minimum value $k_{pv}^{\min}$ of the voltage controller proportional parameter k_{pv} needed for small-signal stability. This can be achieved by gradually increasing k_{pv} until the eigenvalues λ_1 and λ_2 of the system state matrix $\boldsymbol{A}$ lie on the imaginary axis of the s-plane. Finally, we set the parameter k_{pv} such that $k_{pv} > k_{pv}^{\min}$ and complete the tuning process. Note that the VSM virtual impedance and power control loops are assumed to be well tuned beforehand [6], [7].

Remark 1 (Model-order Reduction of VSM-connected System Caused by Setting $k_{iv} = 0$)**.** In addition to improving the VSM stability, a side benefit of setting $k_{iv} = 0$ is to reduce the model order of the VSM-connected system by two, and consequently, facilitate the VSM modelling and analysis. This is because by setting $k_{iv} = 0$, the two differential equations (16) and (17), which describe the voltage controller dynamics, degenerate into algebraic equations. ∎

IV. CASE STUDIES

In this section, via numerical studies of the system in Fig. 1, we validate the analysis and proposed tuning method for the voltage and current loops, which fully consider the full-order system dynamics. In this way, we show the necessity of leveraging the full-order VSM model for tuning parameters in the voltage and current loops. Note that to ensure a fair
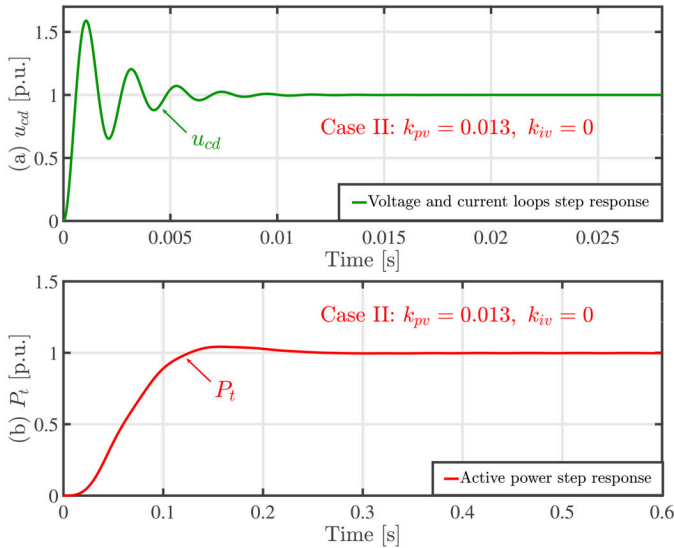
Fig. 7. System dynamics with $k_{pv} = 0.013$ and $k_{iv} = 0$ (case II). (a) Step response of cascaded voltage and current loops in Fig. 3. (b) Active-power step response of the VSM-connected system in Fig. 1

comparison with case I in Example 1, we adopt the same system parameters as reported in Table I, unless otherwise noted.

In the numerical case considered here (case II), we tune the voltage and current loops with the proposed tuning method in Section III-C. Specifically, by setting the current control time constant $\tau_c = 1.0$ ms, we leverage (21) to compute the current controller PI parameters as $k_{pc} = 25$ and $k_{ic} = 1406$. As for the voltage controller, we set the proportional parameter $k_{iv} = 0$, and also, identify that $k_{pv}^{\min} = 0.0057$ results in $\lambda_1 = j0.06969$ and $\lambda_2 = -j0.06969$ along the imaginary axis of the s-plane. Thus, we can select $k_{pv} = 0.013 > k_{pv}^{\min}$ and complete the tuning process.

With the parameters k_{pc}, k_{ic}, k_{pv}, and k_{iv} computed from the proposed method, we first evaluate the step response of the cascaded voltage and current loops in Fig. 3. As plotted in Fig. 7(a), the step response of the voltage and current loops is stable and the settling time turns out to be 8 ms. It is noted that the obtained voltage and current loops settling time is 25 times smaller than the power loop settling time 0.2 s. Thus via comparison with the case I in Example 1, case II here achieves greater time-scale separation as a result of the proposed tuning method. Thereafter, we simulate the VSM-connected system in Fig. 1 in the PSCAD/EMTDC software and plot the active-power step response in Fig. 7(b). We can find that the active power P_t stabilizes at its reference $P_t^\star = 1$ p.u. Also, the settling time of the active-power step response is 0.2 s, which matches our predesigned power loop dynamics precisely. Indeed, for other choices of τ_c within $[0.5, 5]$ ms, the proposed tuning method still leads to stable active-power step responses. In this way, we validate the accuracy of our proposed analysis and tuning method of the cascaded voltage and current loops, which fully consider the full-order system dynamics. Recall that the conventional tuning method in Section II-B, which does not consider the full-order system dynamics, leads to

unstable active-power step response in case I in Example 1. By comparing the stable system dynamics in case II with the unstable ones in case I, we further validate the necessity of considering the full-order VSM-connected system dynamics while analyzing and tuning the voltage and current loops.

V. CONCLUSION

In this paper, via a numerical example, we identified that the conventional voltage and current controller tuning method may not ensure the stability of the VSM-connected system. The root cause is that the conventional method does not consider the full-order VSM dynamics. Thus, we proposed an updated voltage and current controller tuning method, which considers the full-order VSM dynamics. Our proposed method ensures the VSM to be small-signal stable and achieves desired time-domain responses. Also, our tuning method significantly facilitates the parameter tuning of the VSM-connected system.

REFERENCES

[1] B. Kroposki *et al.*, "Achieving a 100% renewable grid: Operating electric power systems with extremely high levels of variable renewable energy," *IEEE Power Energy Mag.*, vol. 15, no. 2, pp. 61–73, 2017.
[2] M.-H. Khooban, T. Dragicevic, F. Blaabjerg, and M. Delimar, "Shipboard microgrids: A novel approach to load frequency control," *IEEE Trans. Sustain. Energy*, vol. 9, no. 2, pp. 843–852, 2018.
[3] H. P. Beck and R. Hesse, "Virtual synchronous machine," in *Proc. 9th Int. Conf. EPQU*, 2007, pp. 1–6.
[4] S. D'Arco, J. A. Suul, and O. B. Fosso, "Automatic tuning of cascaded controllers for power converters using eigenvalue parametric sensitivities," *IEEE Trans. Ind. Applicat.*, vol. 51, no. 2, pp. 1743–1753, Mar. 2015.
[5] S. Dong and Y. C. Chen, "Adjusting synchronverter dynamic response speed via damping correction loop," *IEEE Trans. Energy Convers.*, vol. 32, no. 2, pp. 608–619, Jun. 2017.
[6] S. Dong and Y. C. Chen, "A method to directly compute synchronverter parameters for desired dynamic response," *IEEE Trans. Energy Convers.*, vol. 33, no. 2, pp. 814–825, Jun. 2018.
[7] S. Dong and C. Chen, "Analysis of feasible synchronverter pole-placement region to facilitate parameter tuning," *IEEE Trans. Energy Convers.*, pp. 1–1, 2021, to be published.
[8] T. Qoria, F. Gruson, F. Colas, X. Guillaud, M.-S. Debry, and T. Prevost, "Tuning of cascaded controllers for robust grid-forming voltage source converter," in *Proc. Power Syst. Comput. Conf. (PSCC)*, 2018, pp. 1–7.
[9] W. Du *et al.*, "A comparative study of two widely used grid-forming droop controls on microgrid small-signal stability," *IEEE J. Emerg. Sel. Topics Power Electron.*, vol. 8, no. 2, pp. 963–975, 2020.
[10] W. Ma, Y. Guan, and B. Zhang, "Active disturbance rejection control based control strategy for virtual synchronous generators," *IEEE Trans. Energy Convers.*, vol. 35, no. 4, pp. 1747–1761, 2020.
[11] Z. Qu, J. C.-H. Peng, H. Yang, and D. Srinivasan, "Modeling and analysis of inner controls effects on damping and synchronizing torque components in vsg-controlled converter," *IEEE Trans. Energy Convers.*, vol. 36, no. 1, pp. 488–499, 2021.
[12] S. Eberlein and K. Rudion, "Small-signal stability modelling, sensitivity analysis and optimization of droop controlled inverters in lv microgrids," *Int. J. Electr. Power Energy Syst.*, vol. 125, p. 106404, 2021.
[13] Y. Lin *et al.*, "Research roadmap on grid-forming inverters," National Renewable Energy Lab.(NREL), Golden, CO (United States), Tech. Rep., 2020.
[14] R. Rosso, X. Wang, M. Liserre, X. Lu, and S. Engelken, "Grid-forming converters: Control approaches, grid-synchronization, and future trends - a review," *IEEE Open J. Ind. Appl.*, pp. 1–1, 2021, to be published.
[15] A. Yazdani and R. Iravani, *Voltage-sourced converters in power systems: modeling, control, and applications.* NJ: Wiley, 2010.
[16] C. Zheng, T. Dragičević, and F. Blaabjerg, "Model predictive control-based virtual inertia emulator for an islanded alternating current microgrid," *IEEE Trans. Ind. Electron.*, vol. 68, no. 8, pp. 7167–7177, 2021.
[17] F. Golnaraghi and B. Kuo, *Automatic Control Systems*, 9th ed. New York: Wiley, 2010.